Development of a novel flamelet-based model to include preferential diffusion effects in autoignition of CH4/H2 flames

Abtahizadeh, E. , de Goey, P. and van Oijen, J.

Original citation & hyperlink:
Abtahizadeh, E. , de Goey, P. and van Oijen, J. (2015) Development of a novel flamelet-based model to include preferential diffusion effects in autoignition of CH4/H2 flames. Combustion and Flame, volume 162 (11): 4358–4369
http://dx.doi.org/10.1016/j.combustflame.2015.06.015

DOI 10.1016/j.combustflame.2015.06.015
ISSN 0010-2180
ESSN 1556-2921

Publisher: Elsevier

Development of a novel flamelet-based model to include preferential diffusion effects in autoignition of CH4/H2 flames

Ebrahim Abtahizadeh*, Philip de Goey, Jeroen van Oijen

[a] *Combustion Technology, Mechanical Engineering, Eindhoven University of Technology, 5600 MB Eindhoven, The Netherlands*

Abstract

This study reports on the development of a flamelet-based reduction method for autoignition of hydrogen enriched methane-based fuels. The main focus is on the inclusion of preferential diffusion effects in the Flamelet Generated Manifolds (FGM) technique for autoigniting flames. Such a development of the FGM methodology is inevitable since investigations with detailed chemistry indicate that preferential diffusion strongly affects autoignition of these mixtures. First, a novel flamelet configuration based on Igniting Mixing Layer (IML) flamelets is proposed to accommodate preferential diffusion in a flamelet database. At the next stage, transport equations for controlling variables are derived with additional terms to account for preferential diffusion effects. The extended FGM model has been evaluated by comparing its predictions with those of detailed chemistry in both laminar and turbulent situations. In laminar situations, it is revealed that the model is able to predict accurately autoignition time scales of one-dimensional hydrogen enriched flames. The turbulent situations are studied by performing Direct Numerical Simulations (DNS) of a two-dimensional unsteady mixing layer. In this configuration, the proposed model yields a precise prediction of autoignition time scales as well. The model has also been assessed using the widely used Igniting Counter-Flow (ICF) flamelets instead of IML flamelets which leads to less accurate predictions especially at high hydrogen contents. The predictive power of the proposed model combined with simplicity of its implementation introduces an attractive reduced model for the computation of turbulent flames.

Keywords: Flamelet Generated Manifolds, Preferential diffusion, Autoignition, MILD combustion, Turbulent combustion

1. Introduction

Autoignition of a fuel mixture by a hot oxidizer plays an important role in several new combustion concepts and technologies, e.g. HiTAC, Flox and MILD combustion. These concepts, to which we

*corresponding author

Email address: e.abtahizadeh@tue.nl (Ebrahim Abtahizadeh)

will refer as MILD combustion, have been introduced as promising technologies due to an increased thermal efficiency and decreased pollutant formation [1, 2]. In spite of the enormous potential of the MILD combustion regime, it has been mainly limited to lab-scale burners due to stabilization issues in practical burners. The stabilization mechanism of MILD combustion is often governed by autoignition of a fuel jet in a hot and diluted environment. This mechanism is highly sensitive to variations in the fuel and oxidizer composition and operating conditions. In the experiments by Dally *et al.*, for instance, hydrogen was added to the fuel in order to improve the stabilization [3]. Numerical modeling of MILD combustion of hydrogen rich fuel mixtures poses a significant technical and research challenges due to the complexity of autoignition under large preferential diffusion effects.

MILD combustion can be realized in many configurations depending on preheating and dilution of fuel and/or oxidizer streams. A few examples of this can be found in previous works of de Joannon et al. such as in Hot-Fuel-Diluted-Fuel [4], Hot-Oxidant-Diluted-Fuel [5] and Hot Oxidant Diluted Oxidant [6]. A number of experimental studies has been performed to study the Jet-in-Hot Coflow (JHC) burner as a model system for MILD combustion [3, 7–9]. In most of these experiments, a turbulent lifted flame is observed in a hot environment of oxidizer diluted with burned gas. Recently, hydrogen enriched natural gas flames in JHC burners have been investigated systematically in the experiments of Arteaga *et al.* [10] on the Delft Jet-in-Hot Coflow (DJHC) burner. They observed that the addition of H_2 has a large influence on the lift-off height and stabilization mechanism of these lifted flames. The addition of only 5% H_2 resulted in a more than 50% reduction of the lift-off height. This effect cannot be explained by the change in autoignition delay of homogeneous mixtures due to H_2 addition.

Recent direct numerical simulations of autoigniting mixing layers of CH_4/H_2 mixtures with detailed chemistry and transport models by van Oijen [11] have shed some light to this issue. It was shown that the presence of hydrogen enhances the role of molecular diffusion due to the fact that H_2 diffuses out of the fuel mixture into the hot oxidizer due to its significant preferential diffusion. This leads to a much faster ignition process governed by hydrogen chemistry. However, there is still little knowledge available about the complex role of preferential diffusion in large scale reacting flows.

Numerical modeling of H_2 enriched MILD combustion in the large scale flows, as in the DJHC burner, requires reduced models for turbulence and chemistry. These models should be able to predict adequately complex autoignition events under large preferential diffusion effects. Successful reduction techniques to accommodate preferential diffusion are mainly based on flamelets [12], such as FGM (Flamelet Generated Manifolds) [13], FPV (Flamelet Progress Variable) [14] and REDIM (Reaction-Diffusion Manifolds) [15]. Inclusion of preferential diffusion in FGM has been studied by van Oijen

et al. [13] and later on by de Swart et al. [16] in the context of premixed flames. It has been shown that two controlling variables are needed to account for local variations in equivalence ratio and mass burning rate. Preferential diffusion in the context of non-premixed flames has been taken into account by Pitsch et al. [17, 18]. In their work, a set of flamelet equations was derived with extra terms to account for non-unity Lewis number effects. This model has been used in some studies of turbulent non-premixed flames, for example in [19]. Flamelet-based models were also used to study autoignition in turbulent jet flames (e.g. [20], but the effect of preferential diffusion on ignition was not investigated. To the authors' knowledge, there is no literature about the incorporation of preferential diffusion effects in a flamelet-based technique for autoigniting non-premixed flames.

In part 1 of this two-part paper, the focus is on the extension of the FGM technique to account for preferential diffusion effects in autoignition of CH_4/H_2 mixtures. In section 2, a new type of flamelet called Igniting Mixing Layer (IML) flamelet is introduced with the relevant governing equations. The IML flamelets are analyzed and compared with the commonly used Igniting Counter-Flow diffusion flamelets (ICF flamelets) in terms of preferential diffusion effects in section 3. In section 4, the tabulation of the IML flamelets is discussed. In section 5, an appropriate set of transport equations for the controlling variables is derived to account for non-unity Lewis number effects. The performance of the proposed FGM model is evaluated and validated by comparison with predictions of detailed chemistry first in laminar one-dimensional configuration in section 6 and afterwards, in turbulent two-dimenstional situations in section 7. Finally, conclusions are drawn. Part 2 as a separate paper consists of application of the proposed FGM model based on IML flamelets in LES of the Delft JHC burner. The main purpose of part 2 is to evaluate influence of preferential diffusion effects on the lift-off height and stabilization mechanism of lifted flames.

2. IML flamelets

In this paper, we aim to develop a flamelet model that can predict the effect of preferential diffusion on autoignition of methane-hydrogen mixtures at the conditions in JHC experiments. In total, four cases are studied containing 0 to 25 percent of H_2 by volume, which are summarized in Table 1. These cases correspond to the mean boundary conditions of the DJHC burner experiments [10]. In these experiments, the fuel and oxidizer streams are initially separated. Once the fuel is injected into the hot oxidizer stream, mixing starts, which is then followed by autoignition. Igniting Mixing Layer flamelets (IML flamelets) are introduced here to model this process of mixing and autoignition such as in the DJHC burner. IML flamelets are basically similar to the commonly used one-dimensional Igniting Counter-Flow diffusion flamelets (ICF flamelets) with a notable distinction in the initial condition and

Table 1: Temperature and molar composition of the fuel stream for the different cases. The oxidizer stream has the same composition for all cases: $T = 1437$ K, $X_{O_2} = 0.0485$, $X_{H_2O} = 0.1452$, $X_{CO_2} = 0.0727$, $X_{N_2} = 0.7336$. ζ_{st} is the stoichiometric mixture fraction.

Case	T(K)	X_{H_2}	X_{CH_4}	$X_{C_2H_6}$	X_{N_2}	ζ_{st}
D00H_2	448	0.00	0.813	0.037	0.15	0.0178
D05H_2	448	0.05	0.763	0.037	0.15	0.0179
D10H_2	448	0.10	0.713	0.037	0.15	0.0180
D25H_2	448	0.25	0.563	0.037	0.15	0.0183

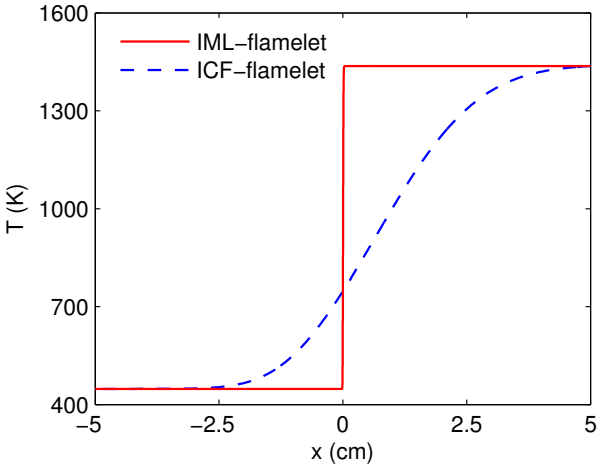

Figure 1: Comparison of the initial temperature profile ($t = 0$ s) between an ICF-flamelet and an IML-flamelet.

inflow momentum. In ICF flamelets, it is a common practice [19–22] to generate an initial condition by assuming a steady-state molecular mixing field between the fuel and oxidizer stream with frozen chemistry ($\dot{\omega} = 0$) as it is shown in Fig. 1. This situation implies that a steady-state mixing field is reached before any chemical reaction takes place. This assumption is mainly valid if the time scale of mixing is much shorter than the chemical time scales. However, such an assumption might lead to unrealistic predictions if molecular diffusion terms are comparable in size to the chemical source terms (for example in H_2-enriched methane mixtures). In this case, molecular diffusion has a large influence on autoignition time scales. This situation is extensively discussed in section 3.

In IML flamelets, in contrast to ICF flamelets, fuel and oxidizer streams are initially unmixed as it is shown in Fig. 1. Such an unmixed profile is adopted here to include preferential diffusion effects in the pre-ignition stage. In this situation, the initial thermo-chemical properties have a step-function profile in physical space. Their values are equal to the fuel boundary on one side of the domain ($x < 0$ in Fig. 1) and equal to the oxidizer boundary at the other side ($x > 0$ in Fig. 1). Due to the steep gradient of mixture fraction at the interface, the scalar dissipation rate $\chi = 2D\,(\partial Z/\partial x)^2$ is very large at this point. During the molecular mixing process, the scalar dissipation rate decreases and chemical

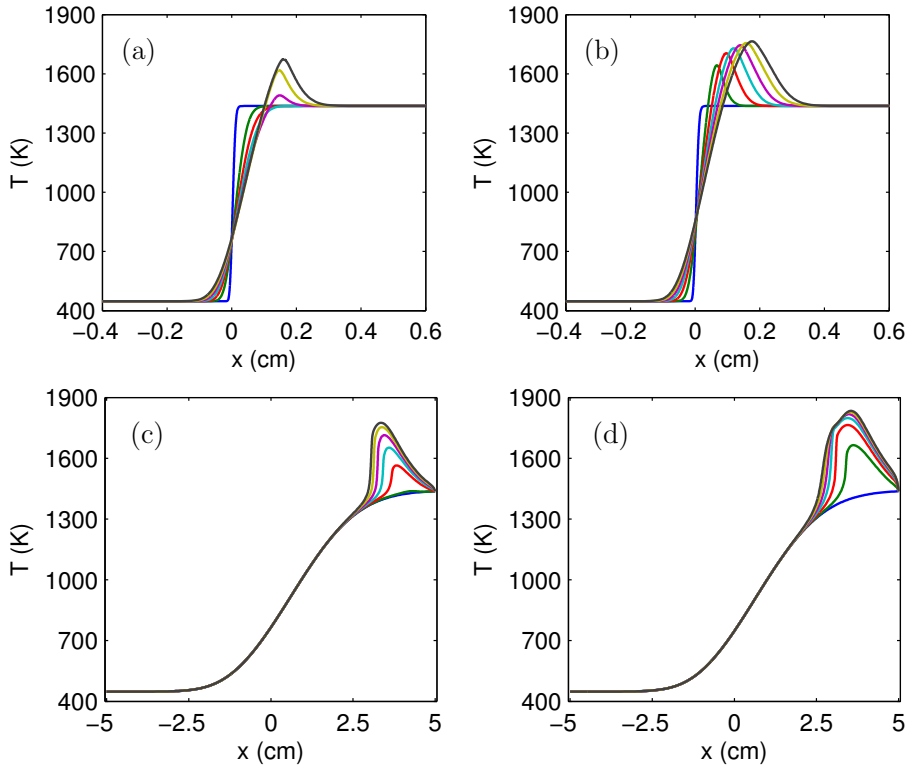

Figure 2: Evolution of temperature for (a) IML flamelets with $\mathrm{Le_i} = 1$, (b) IML flamelets with $\mathrm{Le_i} = \mathrm{c_i}$, (c) ICF flamelets with $\mathrm{Le_i} = 1$ and (d) ICF flamelets with $\mathrm{Le_i} = \mathrm{c_i}$. Case $\mathrm{D25H_2}$, ICF flamelets with $a = 1\ \mathrm{s}^{-1}$. Colored lines refer to flamelets at t = 0, 0.5, 1, ..., 3 ms.

reactions may start at any time during the mixing process. In IML flamelets, the gradient of mixture fraction is not enforced by an inflow momentum (i.e. an applied strain). However, it is governed purely by molecular diffusion. In the absence of an applied strain, the species mass fractions and temperature approach chemical equilibrium for infinite time.

The configuration of IML flamelets resembles practical non-premixed systems in which mixing of the fuel and the oxidizer initiates after their injection from the nozzle exit at very large scalar dissipation rates. In these systems, chemical equilibrium can be reached at a sufficiently large distance from the burner where scalar dissipation rates approach zero.

The mathematical formulation of IML flamelets is described by the following set of one-dimensional transport equations:

$$\frac{\partial \rho}{\partial t} + \frac{\partial \rho u}{\partial x} = 0 \tag{1}$$

$$\frac{\partial (\rho Y_i)}{\partial t} + \frac{\partial (\rho u Y_i)}{\partial x} = \frac{\partial}{\partial x}\left(\frac{\lambda}{Le_i c_p}\frac{\partial Y_i}{\partial x}\right) + \dot{\omega}_i \tag{2}$$

$$\frac{\partial (\rho h)}{\partial t} + \frac{\partial (\rho u h)}{\partial x} - \frac{\partial}{\partial x}\left(\frac{\lambda}{c_p}\frac{\partial h}{\partial x}\right) = \frac{\partial}{\partial x}\left[\frac{\lambda}{c_p}\sum_{i=1}^{N_s}\left(\frac{1}{Le_i} - 1\right) h_i \frac{\partial Y_i}{\partial x}\right] \tag{3}$$

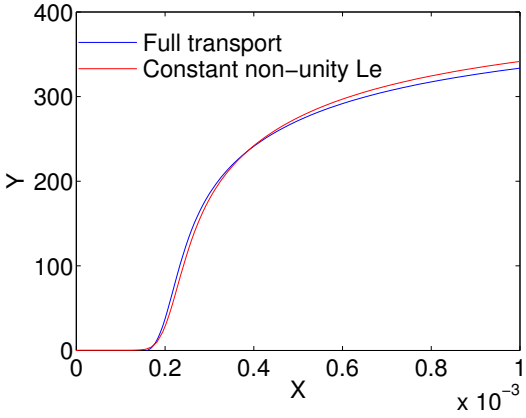

Figure 3: Comparison of the temperature rise ΔT of a one-dimensional igniting mixing layer using detailed chemistry and (blue) full multi-component transport including Soret and Dufour effects and (red) constant non-unity Lewis numbers for the Case D25H2.

with initial condition for $Y_i(x,t)$, $h(x,t)$ and $u(x,t)$ as:

$$Y_i(x,0) = \begin{cases} Y_{i,fu} & \text{if } x < 0 \\ Y_{i,ox} & \text{if } x \geq 0 \end{cases}, \qquad h(x,0) = \begin{cases} h_{fu} & \text{if } x < 0 \\ h_{ox} & \text{if } x \geq 0 \end{cases}, \qquad u(x,0) = 0 \tag{4}$$

where u, h, x and t represent velocity, total enthalpy, distance and time, respectively. ρ, λ, c_p and Le_i refer to mixture density, thermal conductivity, specific heat at constant pressure and Lewis number of species i, respectively. Y_i, $\dot{\omega}_i$ and N_s refer to mass fraction of the i-th species, chemical production rate and total number of species present in the chemical scheme, respectively. The transport model, which is used in these equations to model diffusion of species, is based on assuming constant non-unity Lewis numbers. This model takes into account preferential diffusion effects. Since the full multi-component transport [23] is not used, a velocity correction is applied to the mass fraction of the abundant species (N_2 in this study) in order to ensure mass conservation:

$$Y_{N_2} = 1 - \sum_{i \neq N_2} Y_i \tag{5}$$

This is the same as assuming that the diffusion flux of N_2 is equal to the sum of diffusion fluxes of the other species:

$$\rho u_{N_2} Y_{N_2} = - \sum_{i \neq N_2} \rho u_i Y_i \tag{6}$$

This implies that the Lewis number of N_2 is not necessarily constant and follows from:

$$\rho u_{N_2} Y_{N_2} = - \frac{1}{Le_{N_2}} \frac{\lambda}{c_p} \frac{\partial Y_{N_2}}{\partial x} \tag{7}$$

This methodology for correction of the diffusion velocities works well in flames that are well diluted with N_2 [23]. In our studied cases, there is a considerable amount of N_2 in the oxidizer stream (73%)

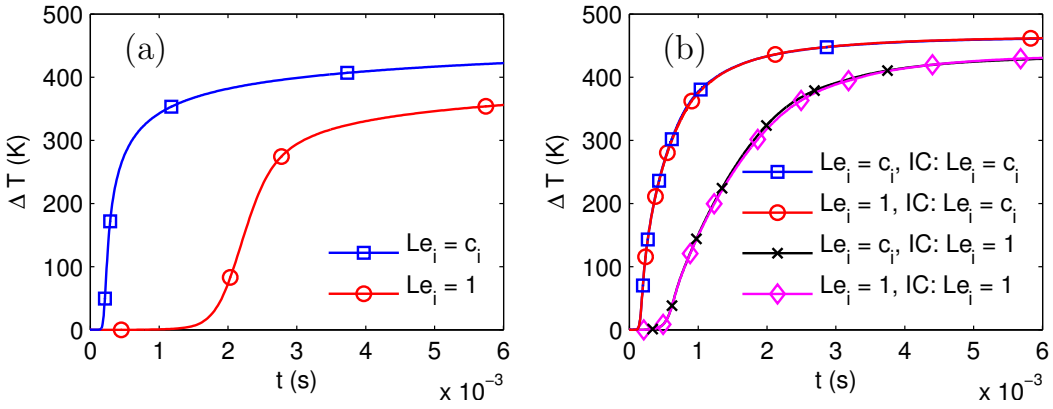

Figure 4: Temperature rise ΔT computed using detailed chemistry and different transport models for (a) IML flamelets and (b) ICF flamelets. In figure (b), different transport models have been used to compute the initial condition (IC) for the ICF flamelets. Case D25H_2, ICF flamelets with $a = 1$ s^{-1}.

as well as in the fuel stream (15%). This correction approach has been shown in our previous works to yield approximately the same results as the full transport model [11, 24]. It is also frequently used by others (e.g. recent DNS studies by Minamoto et al. [25]). In order to demonstrate the accuracy of this approach for the present case with 25% H_2, we have plotted autoignition times obtained by the full multi-component transport including Soret and Dufour effects against those obtained by the constant Lewis numbers approach in Fig. 3. It is observed that the difference between the autoignition time scales is less than 2%. Therefore, it is believed that the correction approach is accurate enough for the present study. The set of governing equations for the IML flamelets is solved by the CHEM1D code which is developed at the Eindhoven University of Technology [24, 26].

3. Analysis of preferential diffusion effects

The effect of preferential diffusion on the autoignition process in the different flamelet types is investigated in this section for the case with the highest H_2 fraction (D25H_2). Figure 2 shows the temporal evolution of temperature in physical space for both IML and ICF flamelets by using detailed chemistry (GRI-mech 3.0) [27] but different diffusion models. In this figure, temperature profiles are shown incrementally in time in which each time level is plotted with a different color. The initial profile is a step-function for the IML flamelets (Fig. 2a and b) while it is a mixed field for the ICF flamelets (Fig. 2c and d). Comparison of the flamelets using unity Lewis numbers ($Le_i = 1$) with those using constant non-unity Lewis numbers ($Le_i = c_i$) reveals that preferential diffusion affects strongly the evolution of temperature for both types of flamelets. The non-unity Lewis numbers for each case are obtained from a simulation of that case with complex multi-component transport. This choice of constant non-unity Lewis numbers ($Le_i = c_i$) is able to predict autoignition time scales as accurate as

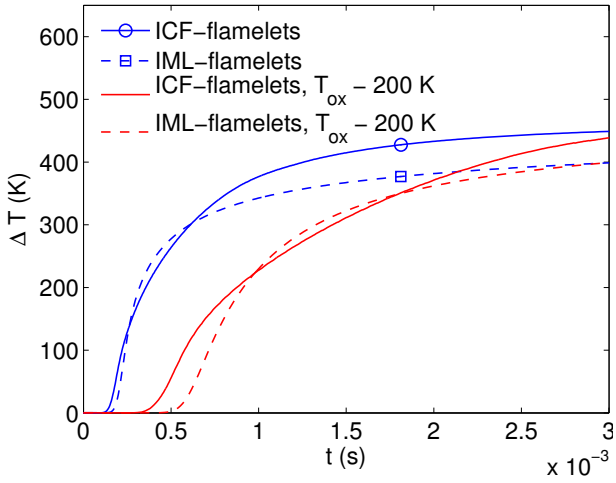

Figure 5: Comparison of the temperature rise ΔT of flamelets using detailed chemistry and $\mathrm{Le_i} = \mathrm{c_i}$ transport at the reference and reduced oxidizer temperatures. Case $\mathrm{D25H_2}$, ICF flamelets with $a = 1\ \mathrm{s}^{-1}$.

the predictions by complex multi-component transport.

A quantitative comparison of the autoignition time scales between the ICF flamelets and IML flamelets is shown in Fig. 4. ΔT represents the maximum temperature rise in mixture fraction ζ space:

$$\Delta T(t) = \max_{\zeta} \left(T(\zeta, t) - T(\zeta, 0) \right). \tag{8}$$

The evolution of ΔT is shown in Fig. 4a for IML flamelets which are computed by using transport models $Le_i = 1$ and $Le_i = c_i$. It is observed that the autoignition time scale of the IML flamelets decreases significantly by inclusion of preferential diffusion effects for the Case $\mathrm{D25H_2}$.

In ICF flamelets, it is possible to use different transport models for the initial profile ($t = 0$ s) and its time evolution ($t > 0$ s). This means that $Le_i = c_i$ transport can be used to generate the initial condition (IC:$Le_i = c_i$) while $Le_i = 1$ is used to compute the evolution from such an initial condition and vice versa. Assuming unity Lewis numbers for the computation of the initial condition leads to linear profiles of Y_i in mixture fraction space, which were used in some previous studies (e.g. [21]). Fig. 4b shows that the autoignition delay time of the ICF flamelets depends solely on the assumed transport model for initial conditions regardless of the transport model used to compute the flamelets. When $Le_i = c_i$ transport is used to generate the initial condition for the ICF flamelets, using both transport models in the actual simulation results in the same autoignition time scale. The same trend can be observed when unity Lewis numbers are used to compute the initial condition (IC:$Le_i = 1$).

Figure 4 also shows that autoignition is delayed for both types of flamelets by assuming unity Lewis numbers. Due to the absence of preferential diffusion, the hydrogen cannot diffuse out of the fuel stream into the hot oxidizer as explained in [11]. The autoignition delay for the IML-flamelet is longer than for the ICF-flamelet, because the scalar dissipation, which has a delaying effect, is much

larger in the IML-flamelet. The IML-flamelet using $Le_i = c_i$ shows a very similar autoignition time scale compared to ICF flamelets with an initial condition based on non-unity Lewis numbers. In both cases, preferential diffusion of hydrogen leads to a very reactive mixture with short chemical time scales. In this case, the large chemical source terms make the influence of the scalar dissipation rate on autoignition negligible.

In order for molecular transport and preferential diffusion to influence autoignition time scales, chemical source terms should be sufficiently small. To support this explanation, a situation is considered in which the chemical source terms are slightly decreased. Figure 5 shows ΔT for both flamelet types in which the oxidizer temperature has been decreased by 200 K. It is observed that at this lower temperature, the ignition delay is longer for both flamelets and that indeed the effect is stronger for the IML flamelet because of the higher scalar dissipation rate in this flamelet type. From these results, it can be concluded that preferential diffusion is mainly important in the pre-ignition phase in which the reactants are mixed. However, once ignition starts after this phase, the chemical source terms become much larger than diffusion terms, which minimize the effect of molecular diffusion.

4. Tabulation of IML flamelets

In this section, a methodology is developed to predict autoignition of hydrogen containing fuels using the FGM framework. In this framework, a reacting flow problem is solved using only a small set of partial differential equations instead of the full set of equations for all species. IML flamelets are tabulated to generate a flamelet database which, as discussed in the previous section, takes adequately into account preferential diffusion effects during molecular mixing and autoignition. The most accurate approach to include these preferential diffusion effects is to adopt four controlling variables, which include the independent mass fractions of the chemical elements z_C, z_H, z_O, and enthalpy h. In this study, we try to capture the changing local conditions of the elements by taking into account a minimum number of controlling variables to keep the computational cost low. For this purpose, IML flamelets are stored in a flamelet database (or manifold) using two controlling variables, mixture fraction ζ and a reaction progress variable $\mathcal{Y}$ to account for mixing and reaction, respectively. These controlling variables are defined in such a way that they represent chemistry with a monotonic increasing reaction progress.

The mixture fraction ζ is defined by a linear combination of elemental mass fractions using the weight factors following Bilger's [28] formulation. The mixture fraction is normalized so that it has its minimum and maximum value in the oxidizer ($\zeta = 0$) and fuel ($\zeta = 1$), respectively. Using these

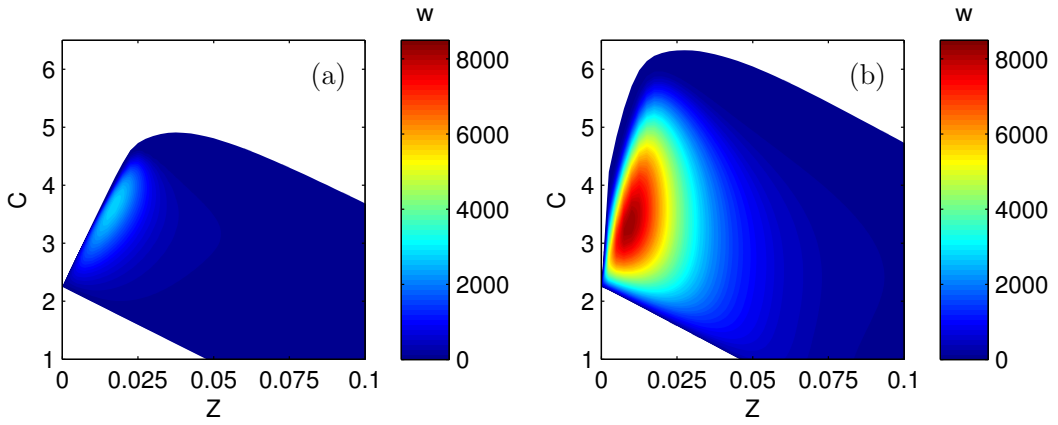

Figure 6: Chemical source term of reaction progress $\dot{\omega}_{\mathcal{Y}}$ as a function of mixture fraction ζ and reaction progress $\mathcal{Y}$. The manifold is created with IML flamelets using (a) $Le_i = 1$ and (b) $Le_i = c_i$.

definitions, ζ can be written as linear combination of species mass fractions

$$\zeta = \sum_{i=1}^{N_s} \beta_i Y_i. \tag{9}$$

The reaction progress variable, in general, has the form of:

$$\mathcal{Y} = \sum_{i=1}^{N_s} \alpha_i Y_i \tag{10}$$

in which α_i denotes the weight factors which are optimized to yield a smooth mapping of all variables with respect to the controlling variables. Here, the coefficients are chosen as $\alpha_{O_2} = -0.5/W_{O_2}$, $\alpha_{CH_4}/W_{CH_4} = -0.5$, $\alpha_{CO_2} = -0.8/W_{CO_2}$, $\alpha_{H_2O}/W_{H_2O} = 1$, $\alpha_{C_2H_6}/W_{C_2H_6} = -3$, in which W_i denotes the molar mass of species i. $\alpha_i = 0$ for all other species. This combination yields a monotonic increasing value of the reaction progress with time for all ζ. Note that this progress variable is not normalized and has non-zero values in the frozen mixing limit. In literature, there are more systematic methods to select the progress variable such as [29–31]. We found that, as we will see in the following, the current choice yields accurate results for autoignition time scales compared with detailed chemistry predictions.

Figure 6 shows a contour plot of the source term of the reaction progress $\dot{\omega}_{\mathcal{Y}}$ in the manifold using IML flamelets with $Le_i = 1$ and $Le_i = c_i$ transport, respectively. An interesting observation is that there is a significant influence of preferential diffusion on the distribution and magnitude of the source term. The manifold which is generated by $Le_i = c_i$ has an approximately two times higher peak source term. This might lead to significant differences when these flamelet databases are used in flame simulations. It should be noted that implemetation of such an IML manifold which has infinite gradients in the initial profile can raise numerical instability issues. To avoid such issues, first, we

performed a time-dependent simulation from such a sharp profile with frozen chemistry for a very small time period (5 μs) in order to slightly smoothen the initial flamelet for the manifold. Afterwards, we used an adaptive meshing scheme in order to have enough number of grid points in that profile.

5. Derivation of transport equations for the controlling variables

When a flamelet database is used in a flame simulation, transport equations for the controlling variables (ζ and $\mathcal{Y}$) have to be solved. All other thermo-chemical variables can be retrieved from the database. In order to derive a transport equation for the reaction progress, we consider the conservation equation for species assuming Fick-like diffusion:

$$\frac{\partial \rho Y_i}{\partial t} + \nabla \cdot (\rho u Y_i) = \nabla \cdot \left(\frac{\lambda}{Le_i c_p} \nabla Y_i \right) + \dot{\omega}_i. \tag{11}$$

By splitting the contribution of species diffusion into non-preferential diffusion and preferential diffusion parts, Eq. (11) reads:

$$\frac{\partial \rho Y_i}{\partial t} + \nabla \cdot (\rho u Y_i) - \nabla \cdot \left(\frac{\lambda}{c_p} \nabla Y_i \right) = \nabla \cdot \left(\frac{\lambda}{c_p} \left(\frac{1}{Le_i} - 1 \right) \nabla Y_i \right) + \dot{\omega}_i. \tag{12}$$

A transport equation for $\mathcal{Y}$ is obtained by taking a linear combination of Eq. (12) using Eq. (10):

$$\frac{\partial \rho \mathcal{Y}}{\partial t} + \nabla \cdot (\rho u \mathcal{Y}) - \nabla \cdot \left(\frac{\lambda}{c_p} \nabla \mathcal{Y} \right) = \nabla \cdot \left(\frac{\lambda}{c_p} \sum_{i=1}^{N_s} \alpha_i \left(\frac{1}{Le_i} - 1 \right) \nabla Y_i \right) + \dot{\omega}_{\mathcal{Y}} \tag{13}$$

A similar transport equation for the mixture fraction is derived using Eqs. (12) and Eq. (9):

$$\frac{\partial \rho \zeta}{\partial t} + \nabla \cdot (\rho u \zeta) - \nabla \cdot \left(\frac{\lambda}{c_p} \nabla \zeta \right) = \nabla \cdot \left(\frac{\lambda}{c_p} \sum_{i=1}^{N_s} \beta_i \left(\frac{1}{Le_i} - 1 \right) \nabla Y_i \right). \tag{14}$$

Note that Eq. (14) does not have a source term and the conservation equation for ζ is only governed by convection, diffusion and accumulation.

Application of non-unity Lewis number transport leads to non-zero transport terms on the r.h.s. of Eqs. (13) and (14). These terms, which contain gradients of $Y_i(\mathcal{Y}, \zeta)$, are derived by using the chain rule:

$$\nabla \cdot \left(\frac{\lambda}{c_p} \sum_{i=1}^{N_s} \gamma_i \left(\frac{1}{Le_i} - 1 \right) \nabla Y_i \right) = \nabla \cdot \left\{ \frac{\lambda}{c_p} \sum_{i=1}^{N_s} \gamma_i \left(\frac{1}{Le_i} - 1 \right) \left[\left(\frac{\partial Y_i}{\partial \mathcal{Y}} \right)_{\zeta} \nabla \mathcal{Y} + \left(\frac{\partial Y_i}{\partial \zeta} \right)_{\mathcal{Y}} \nabla \zeta \right] \right\}, \tag{15}$$

in which γ_i refers to the α_i and β_i coefficients in Eqs. (13) and (14), respectively. Substitution of Eq. (15) in Eqs. (13) and (14) yields:

$$\frac{\partial \rho \zeta}{\partial t} + \nabla \cdot (\rho u \zeta) - \nabla \cdot \left(\frac{\lambda}{c_p} \nabla \zeta \right) = \nabla \cdot \left(\Lambda_{\zeta,\zeta} \nabla \zeta + \Lambda_{\zeta,\mathcal{Y}} \nabla \mathcal{Y} \right), \tag{16}$$

$$\frac{\partial \rho \mathcal{Y}}{\partial t} + \nabla \cdot (\rho u \mathcal{Y}) - \nabla \cdot \left(\frac{\lambda}{c_p} \nabla \mathcal{Y} \right) = \nabla \cdot \left(\Lambda_{\mathcal{Y},\zeta} \nabla \zeta + \Lambda_{\mathcal{Y},\mathcal{Y}} \nabla \mathcal{Y} \right) + \dot{\omega}_{\mathcal{Y}}. \tag{17}$$

Table 2: FGM models using different transport models

Model	IML flamelets	Transport equations
FGM A	$Le_i = 1$	$Le_i = 1$
FGM B	$Le_i = c_i$	$Le_i = 1$
FGM C	$Le_i = c_i$	$Le_i = c_i$

Equations (16) and (17) are transport equations for ζ and $\mathcal{Y}$. The r.h.s. of these equations contain preferential diffusion fluxes in which the following coefficients are introduced:

$$\Lambda_{\zeta,\zeta} = \frac{\lambda}{c_p}\sum_{i=1}^{N_s}\beta_i\left(\frac{1}{Le_i}-1\right)\left.\frac{\partial Y_i}{\partial\zeta}\right|_{\mathcal{Y}}, \quad \Lambda_{\zeta,\mathcal{Y}} = \frac{\lambda}{c_p}\sum_{i=1}^{N_s}\beta_i\left(\frac{1}{Le_i}-1\right)\left.\frac{\partial Y_i}{\partial\mathcal{Y}}\right|_{\zeta}, \tag{18}$$

$$\Lambda_{\mathcal{Y},\zeta} = \frac{\lambda}{c_p}\sum_{i=1}^{N_s}\alpha_i\left(\frac{1}{Le_i}-1\right)\left.\frac{\partial Y_i}{\partial\zeta}\right|_{\mathcal{Y}}, \quad \Lambda_{\mathcal{Y},\mathcal{Y}} = \frac{\lambda}{c_p}\sum_{i=1}^{N_s}\alpha_i\left(\frac{1}{Le_i}-1\right)\left.\frac{\partial Y_i}{\partial\mathcal{Y}}\right|_{\zeta}. \tag{19}$$

These diffusion fluxes incorporate preferential diffusion of each controlling variable due to a gradient of itself and the other controlling variable. The diffusion coefficients are obtained from the gradients of species mass fractions in the directions of $\mathcal{Y}$ and ζ in the manifold. The computed coefficients are stored in the manifold as function of the controlling variables $\mathcal{Y}$ and ζ. They are retrieved from the table during solution of the transport equations.

6. Verification of the FGM model in laminar flames

In this section, the FGM model is used to perform simulations of igniting mixing layers and the results are compared with results of the full chemistry model. Three FGM implementations are considered which employ different transport models in the two stages of the FGM computation: 1) creation of the IML-flamelet tables and 2) solving transport equations for the controlling variables. These models are summarized in Table 2. In FGM A, the IML flamelets are generated using unity Lewis numbers ($Le_i = 1$). FGM B and C have been constructed using a $Le_i = c_i$ transport model. In model FGM C, the transport equations for the controlling variables (Eqs. 16 and 17) are solved in their full form including the preferential diffusion terms. Models FGM A and B do not consider these additional terms in the transport equations.

Figure 7a shows a comparison of the predicted temperature rise ΔT for Case D25H$_2$ using detailed chemistry and the various FGM models. The results of the FGM C model, in which $Le_i = c_i$ is used for both flamelets and transport equations, agree with the detailed chemistry solution perfectly. Such an agreement is also observed for the temporal evolution of temperature in mixture fraction space in Fig. 7b. The negligible differences are caused by interpolation errors in the manifold during

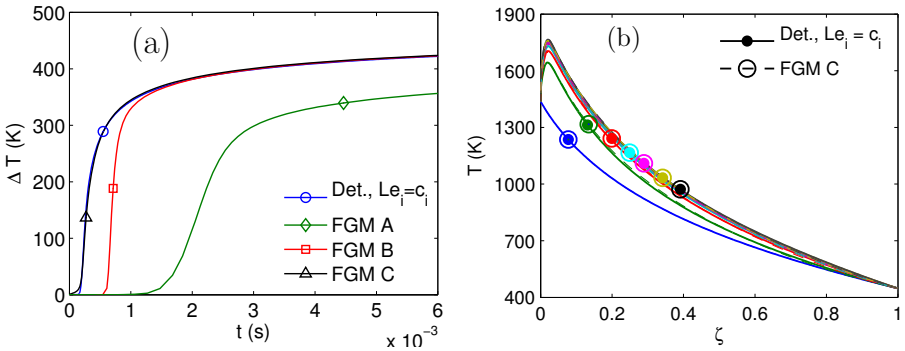

Figure 7: Comparison of (a) temperature rise ΔT and (b) temperature evolution of IML flamelets for the Case D25H_2 with different models. In figure (b), lines with close circles and open circles refer to computations with detailed chemistry and FGM chemistry, respectively.

tabulation of the IML flamelets. When preferential diffusion effects are ignored in both stages of the FGM calculation (FGM A), the ignition delay is almost 10 times longer than the one with detailed simulation. It is interesting to note that compared to FGM A, inclusion of preferential diffusion only in the manifold (FGM B) yields a considerable improvement in the predictions by a factor of four. This is caused by the much higher source terms in the manifold using $Le_i = c_i$ with respect to the manifold using $Le_i = 1$ (cf. Fig. 6).

A similar evaluation of the FGM models is performed for all four cases D00H_2, D05H_2, D10H_2 and D25H_2 in Fig. 8. In this evaluation, the ignition delay τ_{ig} is defined as the time it takes to reach $\Delta T = 50\,\mathrm{K}$, to quantify and compare predicted autoignition time scales. It is observed that the FGM C model, compared to detailed chemistry (Det., $Le_i = c_i$), predicts the ignition delay for all cases perfectly. The FGM A model cannot reproduce these results, but it yields the same ignition delays as the detailed model with unity Lewis numbers. The FGM B model, predicts ignition delays accurately up to 5% hydrogen addition but the agreement deteriorates with increasing hydrogen content in the fuel. However, the FGM B model improves the predictions significantly compared to the FGM A model.

Comparison of the computed ignition delay times of different cases obtained by detailed chemistry in Fig. 8, reveals some interesting points. Including preferential diffusion in the Case D00H_2 increases ignition delay in contrast to the other cases. This can be explained considering the fact that in the Case D00H_2, there is no hydrogen in the fuel mixture. The effect of hydrogen diffusing into the oxidizer stream is therefore absent. However, during the pre-ignition phase, hydrogen molecules and radicals are formed by chain branching reactions. Due to diffusion effects, these species diffuse away from the most reactive mixture fraction ζ_{MR} [32], leading to a decreased reactivity at this location and an increased ignition delay. When non-unity Lewis numbers are applied, the diffusivity of these species

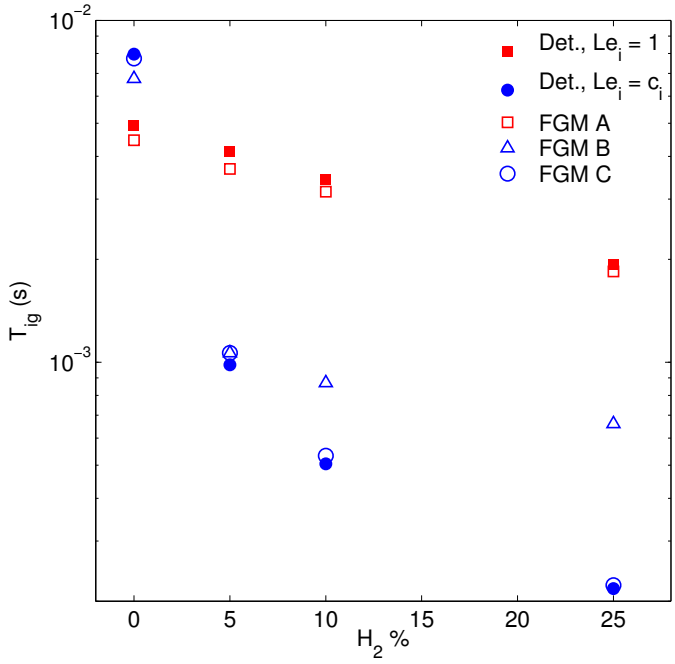

Figure 8: Comparison of ignition delay of IML flamelets for Cases D00H_2, D05H_2, D10H_2 and D25H_2 using detailed chemistry and unity Lewis (Det.Le$_i$ = 1), constant non-unity Lewis (Det.$Le_i = c_i$) with FGM A, B and C models.

(in particular) is enlarged leading to a longer ignition delay.

However, for the other cases, hydrogen is present in the fuel mixture. In these cases, the enhanced diffusion of molecular hydrogen from the fuel to ζ_{MR} leads to a much higher reactivity and shorter ignition delay. Therefore, the ignition delay decreases significantly from 0% H_2 to 5% H_2 in the presence of preferential diffusion.

It is interesting to analyze the influence of each of the four preferential diffusion terms in Eqs. 16 and 17 separately on the predicted autoignition time scales. For this purpose, we define a sensitivity parameter $S_{\tau_{ig}}$ that is computed as follows:

$$S_{\tau_{ig}} = \frac{\Lambda_{i,j}}{\tau_{ig}} \frac{\partial \tau_{ig}}{\partial \Lambda_{i,j}}. \tag{20}$$

To compute the $S_{\tau_{ig}}$, the quantity of each diffusion coefficient, $\Lambda_{i,j}$ in the manifold is multiplied by 0.5 and then, this manifold is used to compute ignition delays. The sensitivity of ignition delay to each of the diffusion flux coefficients is shown in Table 3 for the Case D25H_2. It is clear that ignition delay has the highest sensitivity to $\Lambda_{\mathcal{Y},Z}$ while the sensitivity to the other coefficients is nearly zero. This implies that the diffusion of progress variable by a gradient of mixture fraction accounts for the main preferential diffusion effects.

The application of the developed IML methodology in simulations of turbulent JHC flames has two steps. The first step, which includes creation of an IML manifold by using non-unity Lewis numbers,

Table 3: Sensitivity of ignition delay to diffusion fluxes, Case $D25H_2$

Diff. Fluxes	$S_{\tau_{ig}}$
$\Lambda_{\zeta,\zeta}$	2×10^{-4}
$\Lambda_{\zeta,\mathcal{Y}}$	1×10^{-4}
$\Lambda_{\mathcal{Y},\zeta}$	2.86
$\Lambda_{\mathcal{Y},\mathcal{Y}}$	3×10^{-4}

would be identical to the approach used in this study. The second step, which includes addition of extra terms associated with preferential diffusion to transport equations, is identical for DNS but it requires consideration of turbulence modeling for LES or RANS. This consideration includes filtering or time-averaging of those additional terms for which additional modeling and closures are generally required. In the following section, the IML methodology is applied to the DNS of unsteady mixing layers. Application of this methodology within LES is investigated in the second paper (Part 2) [33] where turbulent flames of a Jet-in-Hot Coflow burner are studied.

7. Application to the 2D DNS of unsteady mixing layers

In this section, the most accurate FGM model (FGM C model) is assessed in an unsteady mixing layer where there is the interaction of flow field with chemistry. For this purpose, Direct Numerical Simulation (DNS) has been carried out in a 2D mixing layer configuration. The relatively simple configuration of 2D mixing layers permits us to perform DNS of autoignition at a reduced computational cost. These mixing layers resemble conditions of JHC burners downstream of the fuel injection point where the fuel stream mixes and ignites in the hot coflow stream.

The employed DNS code solves the conservation equations of mass, momentum, species and energy in a fully compressible form which has been completely explained in [11, 34]. As a brief summary, conservation equations are discretized using a sixth-order finite difference scheme for diffusion terms and the fifth-order for the convective terms. Time integration is performed by an explicit third-order Runge-Kutta scheme. For computations with detailed chemistry, chemical source terms $\dot{\omega}_\alpha$ are computed by using GRI-Mech 3.0 mechanism which includes 53 species and 325 reversible reactions. For FGM chemistry, this solver has been extended here to deal with tabulated chemistry. For this purpose, species equations are substituted by Eqs. (13) and (14) for ζ and $\mathcal{Y}$ in x and y directions. Accordingly, chemical source terms $\dot{\omega}_\mathcal{Y}$ and diffusion coefficients Λ are looked up from the manifold.

DNS is performed for a temporally evolving, non-premixed and planar mixing layer which is shown in Fig. 9. The computational domain is a two-dimensional square with a length of 20 mm consisting of

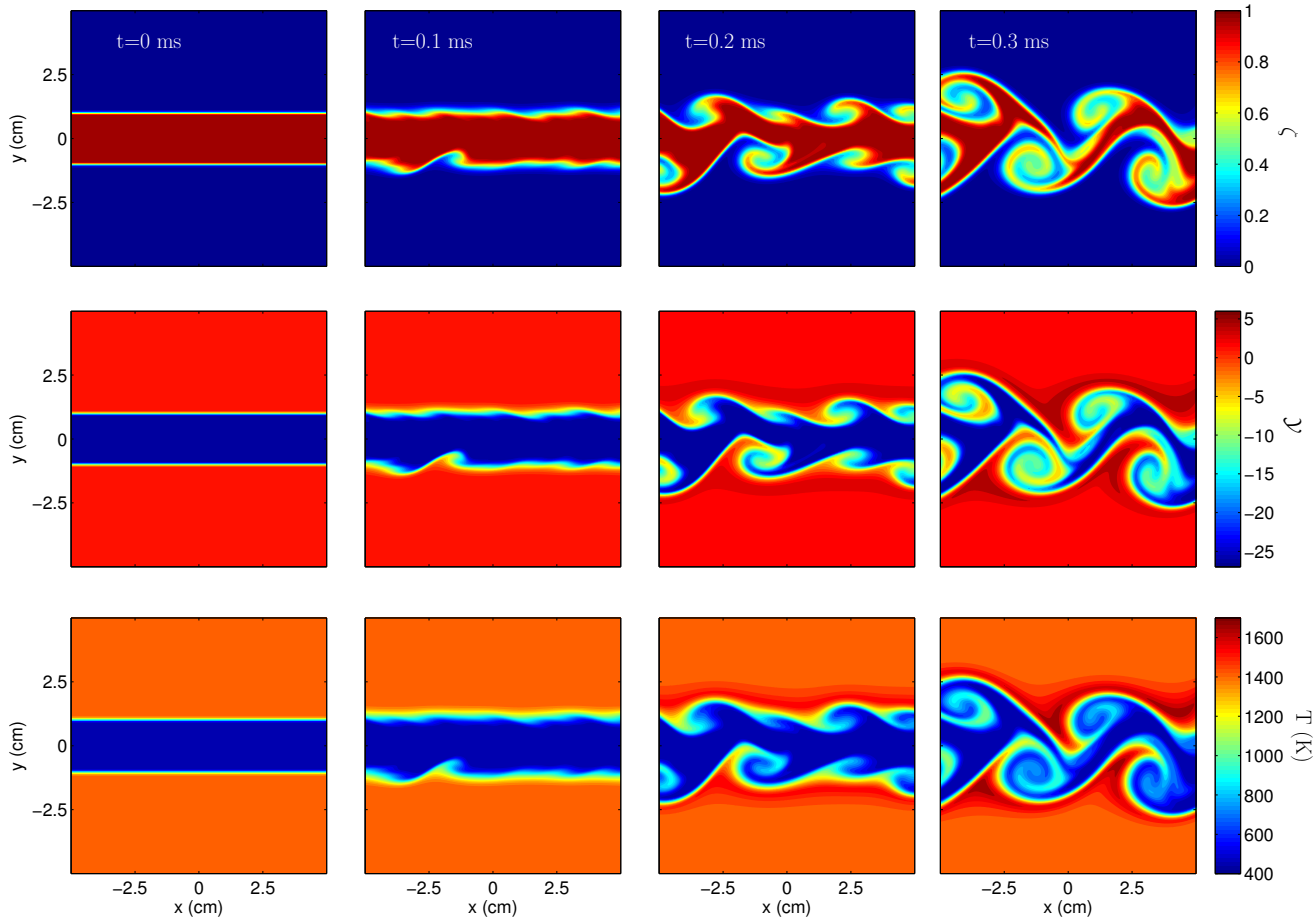

Figure 9: DNS of a 2D mixing layer using detailed chemistry and $Le_i = c_i$ for the Case D25H_2. Figures from top to bottom show time evolution of mixture fraction, progress variable and temperature, respectively.

Table 4: Computed ignition delays τ_{ig} (ms) from simulations of 2D mixing layers by using detailed chemistry and the FGM C model based on IML and ICF manifolds (a $= 100, 300, ..., 10000$ s^{-1}) for the Case D25H$_2$.

Detailed chemistry	ICF manifold						IML manifold
	a = 100s^{-1}	a = 300s^{-1}	a = 500s^{-1}	a = 1100s^{-1}	a = 1500s^{-1}	a = 10000s^{-1}	
0.18	0.37	0.31	0.27	0.23	0.22	0.19	0.19

521 grid points uniformly distributed in each direction which yields a mesh width of 38 μm. Time step is 10^{-8} s which is sufficiently small in order to satisfy the CFL condition. The grid independency check has been performed by using a double number of grid points in each direction for which a negligible deviation has been observed for the ignition delay. Boundary conditions consist of periodic conditions in stream-wise direction and non-reflecting constant pressure in span-wise direction.

In the 2D mixing layer, a layer of relatively cold fuel is surrounded by a hot counter-flowing oxidizer corresponding to boundary conditions given in Table 1. Initially, the fuel layer has a width of 2 mm which is then perturbed by homogeneous isotropic turbulence of low intensity $u'/\Delta U = 1\%$ to trigger the instabilities. The thermo-chemical composition of the initial field corresponds to a top-hat profile in span-wise direction. The Reynolds number of this mixing layer is 3850 which is calculated based on the width of fuel layer, kinematic viscosity of fuel and the relative velocity of the fuel and oxidizer streams ($\Delta U = 67$ m/s). This Reynolds number is in the range of the DJHC experiments ($Re = 4500$) which results in the growth of Kelvin-Helmholtz instabilities in the layer between the fuel and coflow.

ζ, $\mathcal{Y}$ and temperature fields in Fig. 9 show the evolution of mixing and reaction in the mixing layer. These fields are obtained from simulations with detailed chemistry for which ζ, $\mathcal{Y}$ are calculated from species concentrations using Eqs. 9 and 10. It is also observed that the rise of temperature and $\mathcal{Y}$ starts during the growth Kelvin-Helmholtz instabilities between fuel and oxidizer. In this section, the capability of the FGM C model is assessed in the context of such a thermo-chemical evolution of the mixing layer.

Comparison of the temperature rise ΔT obtained from detailed chemistry and the FGM C model is shown in Fig. 10. In the simulations with the FGM C model, three different manifolds are created and used which are either based on IML flamelets (IML manifold) or ICF flamelets (ICF manifold) with a = 100 s^{-1} and 500 s^{-1}. These three manifolds are implemented in the FGM C model to compare predictions of our novel IML manifold with those of the widely-used ICF manifold. The ICF manifold is generated using the ICF flamelets with the same chemical scheme and transport model that have been used to create the IML flamelets. The strain rates that have been applied to ICF flamelets, have the same value for the initial field (t=0) and time-dependent simulations. Comparison of predictions obtained by detailed chemistry with those of the FGM C model reveals that the IML manifold predicts

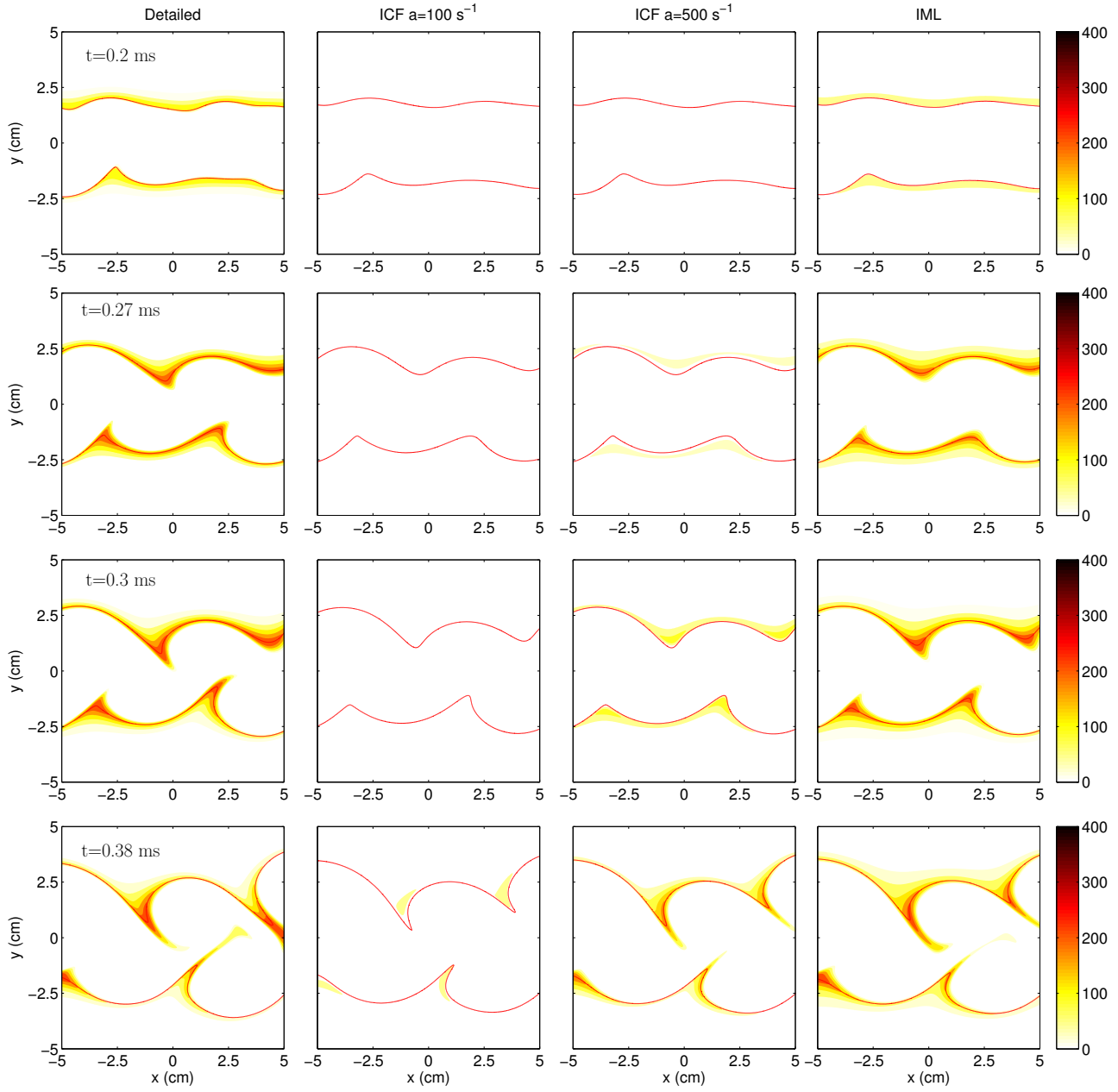

Figure 10: Comparison of the temperature rise ΔT obtained by DNS of 2D mixing layers using detailed chemistry and the FGM C model with IML and two ICF manifolds (a = 100 and 500 s^{-1}) for the Case D25H_2. Red lines correspond to stoichiometric mixture fraction.

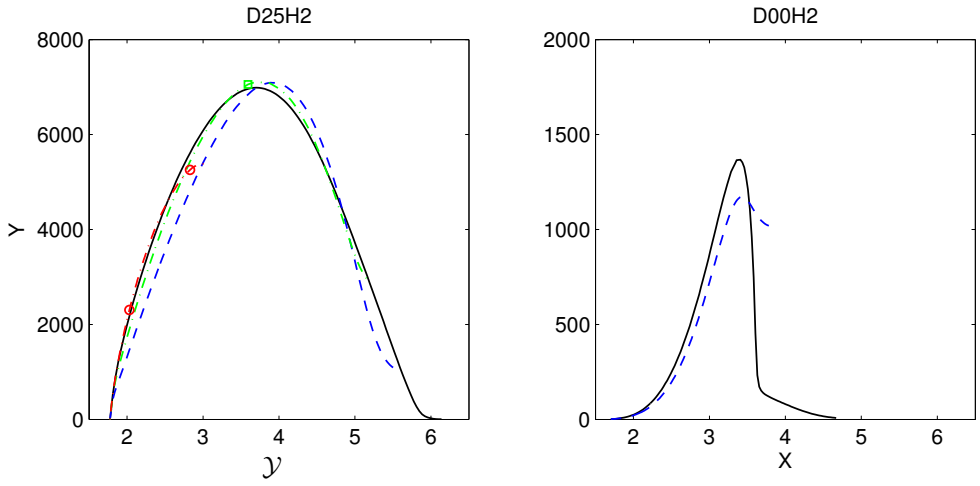

Figure 11: Comparison of $\dot{\omega}_{\mathcal{Y}}$ of (solid line) IML manifold (dashed dotted line with circle) ICF-a10000 Manifold (dashed dotted line with square) ICF-a1500 Manifold (dashed line) ICF-a300 Manifold for all H_2 enriched cases.

the temperature rise much more accurately than the ICF manifold. It is also apparent that predictions with the ICF manifold are improved by increasing the strain rate from 100 s^{-1} to 500 s^{-1}.

Table 4 shows ignition delay of the mixing layer computed by detailed chemistry, the IML manifold and several ICF manifolds with a wide range of strain rates. It is observed that ICF manifolds yield an increasingly improved prediction of ignition delay by increasing of applied strain rate in their flamelets. Although application of the ICF manifold with a very large strain rate ($a = 10000$ s^{-1}) leads to a very good prediction of the ignition delay, it cannot describe complete combustion. This results in a temperature rise of only 70 K at the steady-state condition. However, the IML manifold, which includes an infinite scalar dissipation rate in the initial profile, predicts ignition delay as good as the ICF manifold ($a = 10000$ s^{-1}) while eliminating such incomplete combustion effects.

To investigate the cause of differences between predictions of IML and ICF manifolds, the source terms of $\mathcal{Y}$ are shown in Fig. 11. This figure shows the evolution of $\dot{\omega}_{\mathcal{Y}}$ as a function of $\mathcal{Y}$ at ζ_{st} for Cases D00H_2 and D25H_2. It should be noted that for the Case D00H_2, ICF flamelets do not indicate noticeable autoignition at high strain rates and therefore their $\dot{\omega}_{\mathcal{Y}}$ are not shown in this figure. From Fig. 11, it is observed that the rate of increase of $\dot{\omega}_{\mathcal{Y}}(\mathcal{Y})$ is highest for the IML manifold and also for the ICF manifold with $a = 10000$ s^{-1} while it decreases for other ICF manifolds. Comparison of Fig. 11 with Table 4 demonstrates a direct correlation between the rate of increase of $\dot{\omega}_{\mathcal{Y}}(\mathcal{Y})$ and the predicted autoignition time scales where a higher rate results in a shorter ignition delay and vice versa.

An important observation in Fig. 11 is that although strain rate have a negligible effect on $\dot{\omega}_{\mathcal{Y}}$ of the Case D0H_2, it has a considerable influence on $\dot{\omega}_{\mathcal{Y}}$ of the Case D25H_2. This means that scalar dissipation rate can affect ignition chemistry of H_2 enriched cases. This induces that to include these

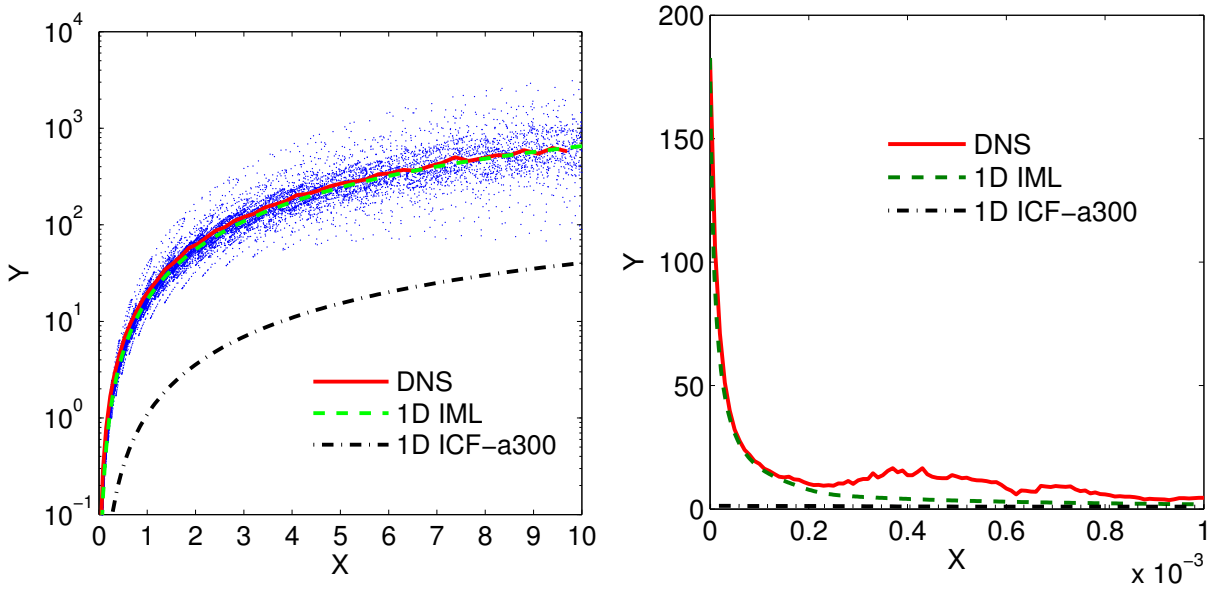

Figure 12: Comparison of scalar dissipation rate between 2D mixing layer, IML and ICF flamelets for the Case D25H_2. Left figure shows (dots) scatter plot of χ and (solid line) its conditional average for the 2D mixing layer compared to χ for (dashed line) IML and (dashed dotted line) ICF flamelets at $t = 0.1$ ms. Right figure shows decay of χ_{st} of the 2D mixing layer, IML and ICF flamelets. In case of the 2D mixing layer, χ_{st} is obtained from conditional averages, detailed chemistry and $Le_i = c_i$.

effects in the ICF manifold an extra dimension would be necessary for H_2 enriched cases. Such an extension of the ICF manifold is not necessary for the Case D00H_2. The reasonably good prediction of autoignition by the IML manifold (cf. Table 4) gives rise to the fact that these effects are incorporated very well in the manifold without the need for an extra dimension. This is due to the fact that the change of scalar dissipation rate follows the same trend in the IML manifold and in the 2D mixing layer.

Figure 12 shows a quantitative comparison of the scalar dissipation rate χ between 1D flamelets and the 2D mixing layer using detailed chemistry. Figure 12a shows a scatter plot of χ and its conditional average obtained from the 2D field compared to χ from IML and ICF flamelets in ζ/ζ_{st} space, all at $t = 0.1$ ms. It appears that the conditional average of χ corresponds very well to χ of the IML flamelet while the ICF flamelet with $a = 300$ s^{-1} shows much lower quantities. Comparison of χ_{st} at different times is shown in Fig. 12b in which χ_{st} for 2D simulations is calculated from the conditional average of the scattered data. χ_{st} is plotted here due to the fact that among different χ values, those found at around ζ_{st}, have the highest impact on ignition delay. From Fig. 12b, it is clear that χ_{st} of IML flamelets decays from a very large value to a small value in a good agreement with that of the 2D mixing layer. However, this trend is not observed for ICF flamelets which indicate nearly constant values at all times.

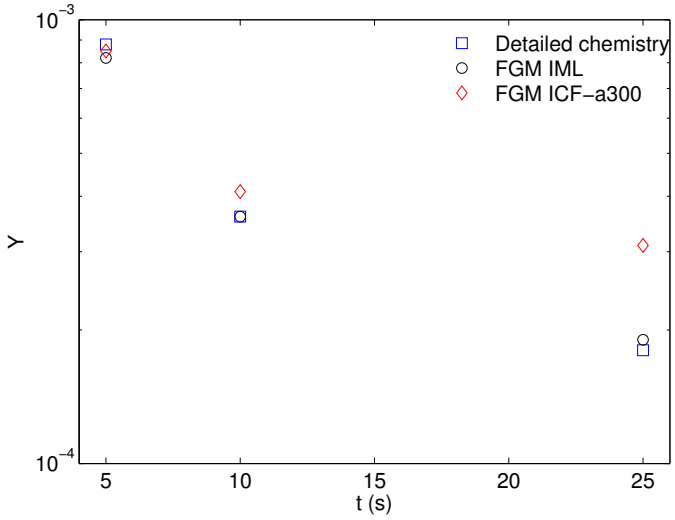

Figure 13: Comparison of ignition delay of 2D mixing layers computed by detailed chemistry and the FGM C model with IML and ICF manifolds for Cases D05H_2, D10H_2 and D25H_2.

It is noticed that there is a small increase in χ_{st} of the DNS around t = 0.4 s. This happens in turbulent situations once turbulent structures from the fuel layer intrude into very lean regions of the stoichiometric mixture fraction Z_{st}. Therefore, they influence scalar dissipation rates in these regions. Such penetrations can more frequently happen for cases that Z_{st} is close to one (fuel side) and the Reynolds number is much larger. Although these effects can be very well included by an additional dimension, it is not necessary to take them always into account. It is noted that these fluctuations happen at t=0.4 ms, much later than the ignition delay at t=0.16 ms. Therefore, if, for instance, the focus is on the prediction of autoignition or lift-off height in lifted flames such as those in JHC burners[10], these effects can be safely neglected.

Comparison of ignition delays obtained from simulations of 2D mixing layers using detailed chemistry and the FGM C model for different H_2 enriched cases is shown in Fig. 13. Ignition delay is computed in the same way as for the 1D flames. The ignition delay is defined as 50 K of maximum temperature rise in mixture fraction space $\Delta T(t) = \max_\zeta(T(\zeta, t) - T(\zeta, 0))$. It appears that at higher hydrogen levels, the application of the IML manifold yields considerably better predictions than the ICF manifold. However, at lower hydrogen contents, the ICF manifold results in accurate predictions as well as the IML manifold. Therefore, it can be concluded that the influence of χ is especially important to create a manifold for cases with significant preferential diffusion.

In summary, the effect of χ on autoignition time scales, which is significant for H_2 enriched cases, is captured very well by IML manifolds because these manifolds include almost the same time history of χ which occurs in 2D mixing layers. This can also possibly be achieved by ICF manifolds but it needs to be extended with an extra dimension to include variation of χ. Another modeling convenience

that is accomplished by using IML manifolds is that its $\dot{\omega}_{\mathcal{Y}}$ approaches zero as $\mathcal{Y}$ reaches its maximum value (cf. Fig. 11). This is, as explained before, due to the fact that scalar dissipation rate approaches zero close to the steady-state and eliminates non-equilibrium conditions. However, for ICF manifolds, equilibrium condition is not reached at the steady-state due to the application of a constant strain rate. This leads $\dot{\omega}_{\mathcal{Y}}$ to end earlier without completing the bell shape. Since one of the main issues in creating a manifold for combustion simulations is to obtain all chemical kinetic information up to the equilibrium condition, IML flamelets provide a straight forward and a relatively easy-to-implement way to generate such a manifold.

8. Conclusions and discussions

A numerical study has been carried out to develop a flamelet-based technique to incorporate preferential diffusion effects in autoigniting flames. Such a development was found unavoidable because investigations with detailed chemistry revealed that preferential diffusion affects strongly the autoignition time scales of H_2-enriched mixtures. IML flamelets were proposed as an adequate flamelet configuration in order to include preferential diffusion effects in molecular mixing and autoignition of the flamelets. IML flamelets with different transport models were tabulated using mixture fraction and progress variables. Transport equations for these controlling variables have been derived with extra terms in order to take into account preferential diffusion. The proposed model has been evaluated in 1D laminar and 2D DNS of unsteady mixing layers. In one-dimensional laminar situations, predictions of autoignition time scales by the FGM C model, which includes preferential diffusion effects in the flamelet database and transport equations, agree very well with detailed chemistry for all studied cases. A sensitivity study revealed that diffusion of the progress variable caused by a gradient of mixture fraction, is the most important preferential diffusion term in the transport equations for the controlling variables. Simplified implementations of the FGM C model were also investigated. It was found that ignoring the preferential diffusion terms in the transport equations yields more deviations for cases with higher H_2 levels. However, for small amounts of hydrogen (5% or less), a good agreement was found with detailed simulations. This simplified model indicates a significant improvement compared to the model where preferential diffusion terms were ignored in both the transport equations and in the manifold creation. The FGM C model provides accurate predctions of autoignition for cases without preferential diffusion effects as well as for those cases with these effects.

This model was further assessed in 2D DNS of unsteady mixing layers. It appears that this model is able to predict autoignition time scales reasonably accurate for all hydrogen enriched cases. It was

observed that the time history of scalar dissipation rate plays an important role for H_2 enriched cases and it influences autoignition. Therefore, the history of scalar dissipation rate χ needs to be taken into account in the manifold. The IML manifold includes the time history of scalar dissipation rate χ similar to the history of χ in the mixing layer of turbulent flames in a Jet-in-Hot coflow burner where χ_{st} decays in time. A manifold based on ICF flamelets with varying χ may also include such a decay but this requires an extra scalar and hence, an additional dimension. This leads to a significantly larger manifold and higher computational costs. The main advantage of IML manifold over the existing methods with an extra dimension for scalar dissipation rate [22, 35] is realized for the case of mixing layer in which scalar dissipation rate decreases during the initial burning stage. This situation is of interest in order to model lift-off height and stabilization mechanism of lifted flames such as those in JHC burners [10]. In these cases, the IML method provides a reduced model which includes approximate representation of the time history of scalar dissipation rate, similar to the existing methods but without the need for that extra dimension. It should be noted that such a decay of χ might not happen in turbulent flames with Z_{st} close to the rich side (fuel layer) and/or with much larger Reynolds numbers. In these conditions, turbulent structures might intrude stoichiometric mixture fractions resulting in an increase or fluctuation of χ_{st}. In these situations, using the extra scalar to account for the variation of χ_{st} might yield more accurate results. This remains to be investigated as a future study. However, in conditions of JHC burners in which the Z_{st} is very close to the lean side ($Z_{st} = 0.0185$) and the Reynolds numbers are not very large (below 10000), application of IML methodology yields accurate predictions. The proposed model provides a relatively easy-to-implement and computationally cost-effective method to be used in simulations of, for instance, jet-in-hot coflow flames which are studied in detail in part 2 [33].

Acknowledgments

The authors gratefully acknowledge the financial support of the Dutch Technology Foundation (STW) under project No. 10414.

References

[1] A. Cavaliere, M. de Joannon, Prog. Energy Combust. Sci. 30 (2004) 329–366.

[2] J.A. Wunning, J.G. Wunning, Prog. Energy Combust. Sci. 23 (1997) 81–94.

[3] B.B. Dally, A.N. Karpetis, R.S. Barlow, Proc. Combust. Inst. 29 (2002) 1147-54.

[4] M. de Joannon, G. Sorrentino, A. Cavaliere, Combustion and Flame 159 (2012), 1832–1839.

[5] M. de Joannon, P. Sabia, G. Sorrentino, A. Cavaliere Proc. Combust. Inst., 2 (2008), pp. 3147–3154.

[6] M. de Joannon, P. Sabia, G. Cozzolino, G. Sorrentino, A. Cavaliere Combust. Sci. Tech., 184 (2012).

[7] R. L. Gordon, A. R. Masri, E. Mastorakos, Combust. and Flame 155 (2008) 181-195.

[8] R. Cabra, J.Y. Chen, R.W. Dibble, A.N. Karpetis, R.S. Barlow, Combust. Flame 143 (2005) 491–506.

[9] E. Oldenhof, M.J. Tummers, E.H. van Veen, D.J.E.M. Roekaerts, Combust. Flame 157 (2010) 1167-1178.

[10] L.D.A. Arteaga, M.J. Tummers, E.H. van Veen, D.J.E.M. Roekaerts, Proc. Combust. Inst. 35 (2015) 3557-3564.

[11] J.A. van Oijen, Proc. Combust. Inst., 34 (2013) 1163-1171.

[12] N. Peters, Prog. Energy Combust. Sci., 10 (1984) 319-339.

[13] J.A. van Oijen, L.P.H. de Goey, Combust. Sci. and Tech., 161 (2000) 113-137.

[14] M. Ihme, H. Pitsch, Combust. Flame, 155 (2008) 70-89.

[15] U. Maas, S.B. Pope, Combust. Flame, 88 (1992) 239-264.

[16] J.A.M. de Swart, R.J.M. Bastiaans, J.A. van Oijen, L.P.H. de Goey, R.S. Cant, Flow, Turb. Combust. 85 (2010) 473-511.

[17] H. Pitsch, M. Chen, N. Peters, Proc. Combust. Inst. 27 (1998) 1057-64.

[18] H. Pitsch, Combust. Flame 123 (2000) 358-374.

[19] K.K.J. Ranga Dinesh, X. Jiang, J.A. van Oijen, R.J.M. Bastiaans, L.P.H. de Goey, Int. J. Hydrogen Energ. 38 (2013) 4848-4863.

[20] C. Bekdemir, L.M.T. Somers, L.P.H. de Goey, J. Tillou, C. Angelberger, Proc. Combust. Inst., 34 (2013) 3067-3074.

[21] P. Domingo, L. Vervisch, D. Veynante, Combust. Flame 152 (2008) 415-432.

[22] M. Ihme, Y.C. See, Combust. Flame 157 (2010) 1850-1862.

[23] T. Poinsot, D. Veynante, *Theoretical and Numerical Combustion*, 3rd ed. (2012).

[24] E. Abtahizadeh, J. van Oijen, P. de Goey, Combust. Flame 159 (2012) 2155-2165.

[25] Y. Minamoto, N. Swaminathan, S.R. Cant, T. Leung, Combust. Flame 161 (2014) 2801-2814.

[26] L.M.T. Somers, The simulation of flat flames with detailed and reduced chemical models, PhD thesis, Eindhoven University of Technology, Eindhoven, The Netherlands, 1994.

[27] G.P. Smith, D.M. Golden, M. Frenklach, N. W. Moriarty, B. Eiteneer, M. Goldenberg, C.T. Bowman, R.K. Hanson, S. Song, W.C. Gardiner, V.V. Lissianski, and Z. Qin, GRI-Mech 3.0, available at <http://www.me.berkeley.edu/gri_mech/>.

[28] R.W. Bilger, Proc. Combust. Inst. 22 (1989) 475-488.

[29] A. Najafi-Yazdi, B. Cuenot, L. Mongeau, Combust. Flame 159 (2012) 1197-1204

[30] M. Ihme, L. Shunn, J. Zhang, J. of Comput. Phys., 231 (2012) 7715-7721

[31] Y. Niu, L. Vervisch, P.D. Tao, Combust. Flame, 160 (2013) 776-785

[32] E. Mastorakos, Prog. Energy Combust. Sci. 35 (2009) 57-97.

[33] S.E. Abtahizadeh, L.P.H. de Goey, J.A. van Oijen, submitted to Combust. Flame, (2014).

[34] J.A. van Oijen, CTR Annual Research Briefs (2011), 225-236.

[35] B. Cuenot, F. Egolfopoulos, T. Poinsot, Combust. Theor. Model. 4 (2000) 77–97.